Check for updates

View Article Online
View Journal

PCCP

Accepted Manuscript

This article can be cited before page numbers have been issued, to do this please use: H. Qin, A. Shamso, A. Centeno, I. G. Theodorou, A. Mihai, M. P. Ryan and F. Xie, *Phys. Chem. Chem. Phys.*, 2017, DOI: 10.1039/C7CP01959A.

This is an Accepted Manuscript, which has been through the Royal Society of Chemistry peer review process and has been accepted for publication.

Accepted Manuscripts are published online shortly after acceptance, before technical editing, formatting and proof reading. Using this free service, authors can make their results available to the community, in citable form, before we publish the edited article. We will replace this Accepted Manuscript with the edited and formatted Advance Article as soon as it is available.

You can find more information about Accepted Manuscripts in the author guidelines.

Please note that technical editing may introduce minor changes to the text and/or graphics, which may alter content. The journal's standard Terms & Conditions and the ethical guidelines, outlined in our author and reviewer resource centre, still apply. In no event shall the Royal Society of Chemistry be held responsible for any errors or omissions in this Accepted Manuscript or any consequences arising from the use of any information it contains.

ROYAL SOCIETY OF CHEMISTRY

rsc.li/pccp

View Article Online
DOI: 10.1039/C7CP01959A

Journal Name

ARTICLE

Published on 19 June 2017. Downloaded by Imperial College London Library on 23/06/2017 03:50:57.

Received 00th January 20xx,
Accepted 00th January 20xx

DOI: 10.1039/x0xx00000x

www.rsc.org/

Enhancing the Upconversion Photoluminescence of Hexagonal Phase $NaYF_4$:Yb^{3+}, Er^{3+} Nanoparticles by Mesoporous Gold Films

Heng Qin[a], Ahmed E. Shamso[a], Anthony Centeno[b], Ioannis G. Theodorou[a], Andrei P. Mihai[a], Mary P. Ryan[a*], Fang Xie[a*]

Efficient enhancement of photoluminescence in rare-earth activated upconversion materials is of great significance for their practical applications in various fields. In this work, three-dimensional mesoporous gold films were fabricated by a low-cost and facile dealloying approach to improve the upconversion photoluminescence efficiency. The mesoporous Au films exhibit good chemical stability, large-area uniformity and abundant distribution of porous nanospaces. Varying the time of the dealloying process leads to modification of pore size distribution, surface roughness and residual Ag content, resulting in effective tuning the wavelength of the broadband localized surface plasmon resonance (LSPR). Enhancement factors were identified to be a function of the dealloying time. With the optimized upconversion photoluminescence enhancement a 41-fold increase was achieved with the mesoporous gold substrate which had been dealloyed for 8 days. These results pave the way to overcome the limitation of poor upconversion efficiency for widespread practical applications in life sciences and energy applications.

1. Introduction

Research on lanthanide-doped upconversion nanoparticles (UCNPs) has recently attracted considerable attention, driven by their diverse potential applications, including in solar cells, biomedical imaging, solid-state lasers, display technology, and security printing.[1] Upconversion photoluminescence (UCPL) is a nonlinear process, through which one photon at a shorter wavelength is emitted, following successive absorption of two or more photons, at longer wavelengths. Upconversion is one of the most elegant approaches to enhance the performance of all classes of solar cells, and is theoretically predicted to be able to increase the efficiency above the Shockley-Queisser limit.[2] Currently, the dominant losses (about 35%) of solar cell efficiency are due to the sub-band-gap energy losses.[3] An efficient luminescence upconversion system could potentially improve the efficiency of traditional solar cells, by harvesting the otherwise lost sub-band-gap photons in the solar spectrum. However, the efficiency of the most promising upconversion materials, $NaYF_4$ host lattice doped with Yb^{3+}/Er^{3+}, remains low due to the small absorption cross sections arising from formally forbidden *f-level* atomic transitions of the dopants[4]. As a result there is negligible progress in the enhanced performance of devices by incorporating upconversion materials. A very recent report[5] demonstrated a 7.9% power conversion efficiency (PCE) enhancement of perovskite solar cells by placing the upconversion single crystal on the front of the device. Improving the efficiency of UCNPs is urgently needed for their practical applications, especially in solar cells. The emerging field of plasmon-enhanced upconversion is a promising avenue for improving the upconversion efficiency of rare-earth (RE) doped materials. To date, a number of plasmonic geometries such as nanograting[4], disk-coupled dots-on-pillar antenna array[6] and core-shell nanostructure[7,8] have been investigated for enhancing UCPL. These nanostructures lead to the UCPL enhancement from 2.3 times[8], to tens of times[9,10], to about 300 times[6], respectively. In our opinion, the wide range of such enhancement factors being reported are not comparable, as the individual systems reported have different pumping power. In addition, the enhancement factors are also relying on various factors such as the choice of plasmonic materials, the structural morphology, the distance between UCNPs and

[a] Department of Materials and London Centre for Nanotechnology, Imperial College London, Exhibition Road, London SW7 2AZ, United Kingdom
[b] Department of Electrical and Electronic Engineering, Xi'an Jiaotong Liverpool University, 111 Ren'ai Road, Suzhou Dushu Lake Higher Education Town, Jiangsu, China 215123.
[c] E-mail: m.p.ryan@imperial.ac.uk or f.xie@imperial.ac.uk

This journal is © The Royal Society of Chemistry 20xx

Physical Chemistry Chemical Physics Accepted Manuscript

Please do not adjust margins

View Article Online
DOI: 10.1039/C7CP01959A

Published on 19 June 2017. Downloaded by Imperial College London Library on 23/06/2017 03:50:57.

nanostructure surface and the optical properties of UCNPs and plasmonic nanostructures *etc.* However, the difficulties in fabricating high quality plasmonic substrates over a large area, without stringent experimental conditions, still hinder the practical applications of plasmon enhanced upconversion luminescence. In some cases, the plasmons even quenched rather than enhanced emission.[11,12]

In this work, we utilized a three-dimensional (3D) mesoporous gold (Au) film by a free corrosion dealloying process, to enhance the UCPL of hexagonal phase β-$NaYF_4$:Yb^{3+}, Er^{3+} co-doped nanocrystals (Figure 3a). This dealloying approach is effective for producing mesoporous Au substrates with tuneable pores sizes, extended framework. Compared with other reported plasmonic structures, the mesoporous Au films have a large area and uniform distribution of porous nanospaces. Due to the existence of abundant nanospaces, these structures also exhibit high carrier density, provide surfaces with sufficient functional sites and thus fascinating optical properties.[13] Moreover, the fabrication method utilized is low-cost, large-scale and easy to control. In this work, by tuning the pore size of mesoporous Au films, a 41-fold luminescence enhancement over a large area (~1.0 cm^2) was achieved. A localized Surface Plasmon Resonance (LSPR) was measured experimentally at ~550 nm due to the nanopores. To obtain physical insights of UCPL enhancement, both the red emission and green emission lifetimes were measured, together with electromagnetic modelling. It was found that, for green emission (~540 nm), the enhancement was dominated by non-resonant enhancement at the pumping wavelength which increased with increasing pore size. While for red emission (~650 nm), both emission enhancement and field enhancement contributed to the UCPL enhancement.

2. Experimental

2.1 Materials and methods

All reagents were of analytical grade. Yttrium(III) chloride anhydrous powder (YCl_3 99.9%), Erbium(III) chloride anhydrous powder ($ErCl_3$ 99.9%), Ytterbium(III) chloride anhydrous powder ($YbCl_3$ 99.9 Ammonium fluoride (NH_4F ≥99.99% trace metals basis), Sodium hydroxide (NaOH ACS reagent, ≥97.0%, pellets) and 1-Octadecene (technical grade, 90%) was purchased from Sigma-Aldrich. Oleic Acid (OA 70%) was purchased from Fisher Chemical (UK). All alloy silver/gold used in this work was purchased from Sepp Leaf Products (New York). Concentrated nitric acid (HNO_3) (Sigma Aldrich, ACS reagent, ≥90.0%) and 18.2 Megohm-cm Ultrapure water) were used.

2.2 Fabrication of mesoporous gold films

Silver and gold (Ag-Au) alloy films, with the thickness of ~100 nm, were floated on the surface of concentrated nitric acid (HNO_3), based on a method described by Ding et al.,[16] as illustrated in Figure 1. The samples were exposed to the acid solution for different times (1 min, 3 min, 10 min, 30 min, 2 h, 12 h, 24 h, 3 days, or 8 days), to study the effect of dealloying time on the morphology and pore sizes of mesoporous Au film (Figure S6.(a-j)). The leaf was then transferred to ultrapure water for 35 min to completely quench the dissolution and diffusion reactions. The floated films were then "fished" out of the solution on the surface of glass substrates previously coated with an amine self-assembled monolayer, by treating them with 4% v/v APTES (aminopropyltriethoxysilane) in acetone. This amine monolayer has a high affinity to Au atoms, increases adhesion of the Au film to the glass substrate and prevents its delamination during following processing steps. The fished samples were finally allowed to dry in ambient atmosphere and used for morphological and optical characterization, and subsequent fabrication processes.

2.3 Synthesis of β-$NaYF_4$:Yb^{3+}, Er^{3+} UCNPs

In a typical thermal decomposition synthesis process[22,23], chloride-based rare earth precursors Yttrium Chloride (YCl_3 99%), Ytterbium Chloride ($YbCl_3$ 99%), and Erbium Chloride ($ErCl_3$ 99%), were used as a dopants precursor. To fulfil the percentage composition, 0.75 mmol of Yttrium Chloride (YCl_3 99%), 0.064 mmol of Ytterbium Chloride ($YbCl_3$ 99%), and 0.02 mmol of Erbium Chloride ($ErCl_3$ 99%) were all mixed into three-neck round-bottom flask with 4 mL of Oleic Acid (OA) and 15 mL of Octadecene (ODE).

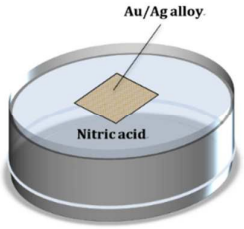

Figure 1. Schematic illustration of the free corrosion dealloying process used to fabricate Au mesoporous films.

All of the mixtures then heated at 150^{0}C in the open environment to remove all of the unnecessary elements such as oxygen and water for 40 minutes. The colour of the mixture should change from soft yellowish cloudy transparent to clear strong yellowish solution. The change of colour indicates that all of the powder precursors had been dissolved completely. Then 2.5 mmol of sodium hydroxide (NaOH) in 5 mL methanol and 4 mmol of ammonium fluoride (NH_4F) in 5 mL methanol were prepared separately and sonicated for about 15 minutes to be fully dissolved. Afterwards, both of them were quickly injected into the dopant solution at room temperature with vigorous stir. After injection sodium hydroxide and ammonium fluoride methanol solution simultaneously, the mixed solution of dopant and crystal host solution was heated up to 50 ^{0}C for 30 minutes under vacuum to remove methanol. Then, the solution was continued to be heated up to 320 ^{0}C under gentle argon gas flow for 90 minutes. Finally, the UCNPs product were washed and centrifuged (4500 r.p.m.) by ethanol and cyclohexane in sequence and was repeated for 3 times,

Physical Chemistry Chemical Physics Accepted Manuscript

This journal is © The Royal Society of Chemistry 20xx

Please do not adjust margins

View Article Online
DOI: 10.1039/C7CP01959A

Published on 19 June 2017. Downloaded by Imperial College London Library on 23/06/2017 03:50:57.

respectively. The colloid of UCNPs in cyclohexane can be stored in a refrigerator (4 °C) for further use.

2.4 Characterisation of UCNPs and Plasmon-Enhanced Upconversion Structure

The particle size, size distribution, phase, and homogeneity of as-synthesized UCNPs were characterized by transmission electron microscopy (JEOL JEM-2100F,) combined with energy-dispersive X-ray spectroscopy (EDX, Oxford Instruments, UK), under an accelerating voltage of 200 kV. In brief, the resulting white precipitates of synthesized UCNPs were dispersed in cyclohexane by ultrasonic sonication for 30 minutes. Several drops of the suspension were drop-casted onto a carbon-coated copper TEM grid. Finally, the samples were allowed to dry in air for 120 minutes and analysed by TEM. Scanning electron microscopy (SEM) was performed using a LEO Gemini 1525 field emission gun (FEG) SEM (Carl Zeiss Microscopy GmbH, UK), to further characterize the phase and phase distribution of UCNPs. The suspension was then drop-casted onto a clean transparent glass substrate. Then, a 10 nm layer of gold (Au) was sputter-coated on the surface of the glass substrate with UCNPs, to inhibit charging and reduce thermal damage. SEM was also used to investigate the surface morphology of Au mesoporous substrates.

2.5 Optical characterization

UV Visible (UV-vis) absorption spectroscopy was performed using the Agilent Cary 5000 UV-Vis-NIR spectroscopy system, to characterize the plasmonic properties of the mesoporous Au films. Glass substrates were used for holding all the samples, as they do not have a restricted wavelength range within our scanning range. Scans were performed over the range from 300-2400 nm, using a scanning rate of 100 nm/min, and a bandwidth of 0.1 nm. The baseline correction was performed using clean glass substrates. All the spectra presented here were obtained using un-polarized light.

2.6 Photoluminescence (PL) Measurements

The fluorescence emission measurements were obtained using a Fluorolog®-3 Spectrofluorometer system) from Horiba Scientific, equipped with a LSR980H steady state laser with adjustable power supply from LASEVER. The angle of acquisition was fixed at 30° for accuracy and consistency of the measurements. The samples were excited by 980 nm NIR light laser excitation with a power density of $500\ \mathrm{mW\cdot cm^{-2}}$ and the upconversion emissions were measured in the range of 450-700 nm, using a 5 nm slit size. The enhancement factor due to the plasmonic Au substrates was estimated using the equation:

$$E = \frac{I_{UC,NPG} - I_{Glass}}{I_{UC,Glass} - I_{Glass}} \qquad (3)$$

Where I is the upconversion photoluminescence intensity obtained from UCNPs coated on top of a mesoporous Au substrate or on a glass reference substrate, while I_{Glass} represents the noise signal from clean glass substrate. This equation does not take into account any corrections for the surface area coverage of the UCNPs. Since our substrates were prepared by the drop casting technique, which means the UCNPs densities on both Au mesoporous film and glass control were identical. This was further confirmed by counting the numbers of UCNPs within the same area on both surfaces of SEM images (Figure 7, Figure S9). Therefore the UCPL enhancement observed is only due to the plasmonic influence of Au mesoporous films.

2.7 Photoluminescence Lifetime measurement

Time-correlated single-photon counting (TCSPC), which is considered as the most sensitive digital technique for determining photoluminescence lifetimes, was applied to obtain dynamic pictures of upconversion photoluminescence of the as-prepared samples.[25] We used the 980 nm pulsed laser to statistically characterize the time dependent photoluminescence emission profiles of the as-synthesized UCNPs by repeating the excitation-emission process up to 5000 counts. The DD-980L laser source has a peak wavelength at 980 ±10 nm, an extremely narrow 100 picosecond pulse width, 0.2 mW power on average and the repetition rate is 50MHz.

3. Results and discussion

3.1 Plasmon-enhanced upconverters

A simple and reproducible plasmonic upconversion structure was fabricated, as illustrated in Figure 2. The structure was composed of four parts: a transparent glass substrate for support, a mesoporous Au layer, followed by an 8 nm SiO_2 spacer layer (thickness was controlled by a sensitive detector of Mantis Deposition System), and a sub-monolayer of the UCNPs on top. The fabrication of mesoporous Au films on glass substrates was based on a free-corrosion dealloying process, which produces continuous Au films with a wide range of tuneable pore sizes.[16, 17, 18] By exposing Au films to a concentrated nitric acid solution for varying times, the morphology and pore size of mesoporous Au films could be modified.[18,19]

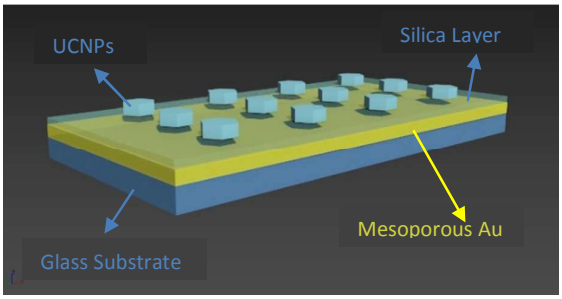

Figure 2. Schematic diagram of the plasmon-enhanced upconversion structure designed and fabricated in this work. The structure was composed of four major components: (i) glass substrate on the bottom, (ii) gold (Au) mesoporous film, (iii) silica (SiO_2) spacer layer, and (iv) β-$NaYF_4$:Yb^{3+} , Er^{3+} UCNPs sub-monolayer.

Physical Chemistry Chemical Physics Accepted Manuscript

Please do not adjust margins

View Article Online
DOI: 10.1039/C7CP01959A

Published on 19 June 2017. Downloaded by Imperial College London Library on 23/06/2017 03:50:57.

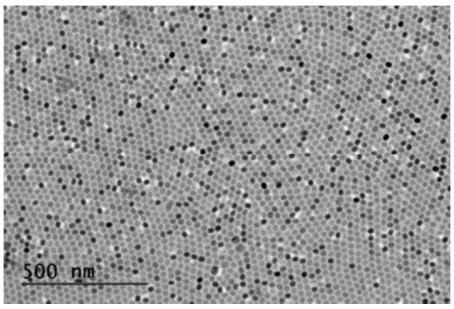

(a)

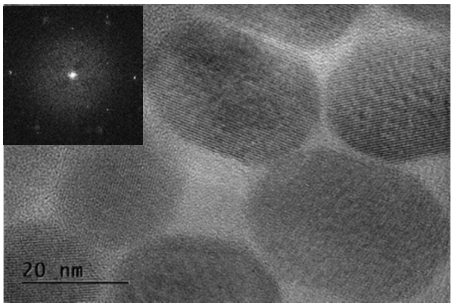

(b)

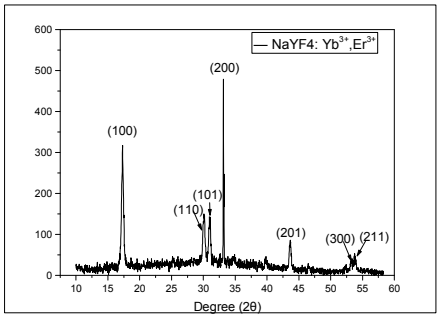

(c)

Figure 3. (a) Transmission electron microscopy (TEM) image of hexagonal β-NaYF4:Yb3+, Er3+ nanocrystals, with a lateral particle size of 25.5±1.4 nm. (b) High resolution (HR) TEM image of UCNPs with 300K magnification. The inset of Figure 3(b) is the live-FFT diagram of the UCNPs. (c) X-ray powder diffraction (XRD) pattern of β-$NaYF_4$:Yb^{3+}, Er^{3+} UCNPs.

3.2 Morphological and compositional analysis of mesoporous Au films

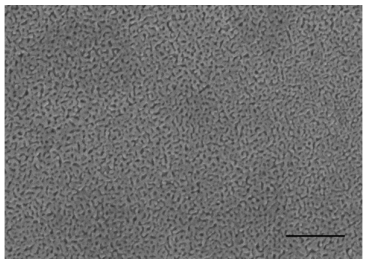

(a)

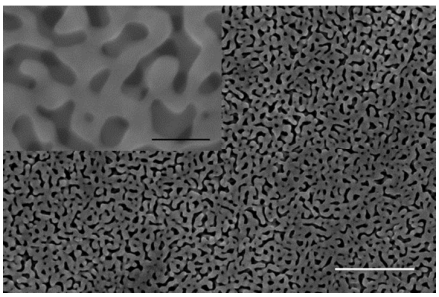

(b)

Figure 4. (a) Top-view SEM micrographs showing the porosity of Au mesoporous film with 2 hours dealloying time (with 500 nm scale bar and 50K magnification). (b) Top-view SEM micrographs showing the porosity of Au mesoporous film with 72 hours dealloying time (with 1000 nm scale bar and 50K magnification). The inset of Figure 4(b) is Au mesoporous film with 72 hours dealloying time with higher magnification (200K). The scalebar in the inset in 150 nm.

When as-received Ag-Au alloy films were floated on the surface of concentrated nitric acid through surface tension, Ag dissolution started immediately, initiating the dealloying process. Dealloying of the films was visually apparent by the change of their colour. SEM imaging revealed the porosity evolution of the films with dealloying time of 1 minutes and 8 days, respectively, which led to an increase in ligament and average pore sizes (Figure 4a, 4b and Figure 5(a)) in agreement with published literature.[19] The average ligament spacing as a function of dealloying time from 1 minutes to 8 days, is shown in Figure S6 in detail. For UCPL enhancement study, we only choose representative four samples, i.e. samples with dealloying times of 3 min, 10 min, 12 hours, and 8 days. The corresponding average pore sizes are 5 nm, 15 nm, 52 nm, and 72 nm, respectively. The significant decrease of Ag content with time due to dissolution results in more pores generated in the structure of Au film. After 3 days of dealloying, the pore size reached its plateaus. The residual Ag content of the mesoporous Au films, which depends on dealloying time, was investigated by SEM-EDX analysis of the entire sample (Figure 5(b)). EDX analysis showed that the Ag content declined rapidly after reaction with HNO_3. In these experiments Ag was not detected for dealloying times greater than 30 min, which could be attributed to the presence of Ag contents lower than the detection limit, but previous work[19] suggests that up to 8% Ag is trapped inside the Au ligaments.

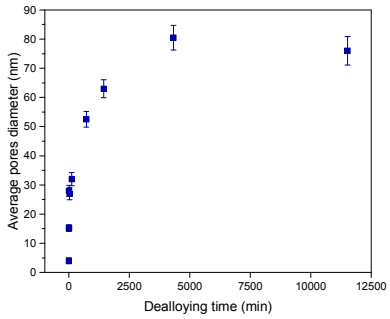

(a)

Physical Chemistry Chemical Physics Accepted Manuscript

This journal is © The Royal Society of Chemistry 20xx

Please do not adjust margins

View Article Online
DOI: 10.1039/C7CP01959A

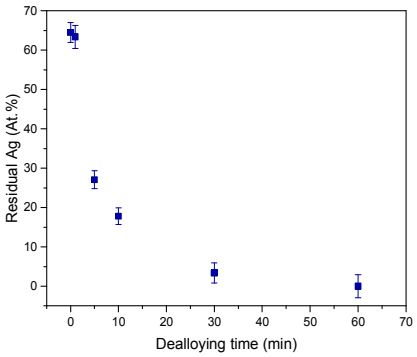

(b)

Figure 5. (a) Average pore size evolution as a function of dealloying time. (b) Residual silver content of Au mesoporous films as a function of dealloying time.

In addition to Ag dissolution, surface diffusion of Au is responsible for the porosity evolution. At the very early stages of reaction, the porous network is not continuous following dealloying times of 1 minutes (Figure S6 (a)) and 3 minutes (Figure S8), and the porosity was not uniformly distributed. As dealloying times increased beyond 5 minutes, the porous structure becomes homogenous and well-developed, and porosity evolution becomes dominated by the surface diffusion processes. A growth in ligament size and spacing was observed, since Au atoms rearrange themselves in such a way to lower their free energy and entropy. Adjusting dealloying process parameters such as the alloy composition, time and temperature enable us to control the surface features of mesoporous Au films for the optimization of their specific performances. The optical properties of mesoporous films are in turn controlled by these resultant surface morphology and chemistry, features that can be tailored by processing time.

3.3 Plasmonic enhancement of β-$NaYF_4$:Yb^{3+} Er^{3+} UCNPs

Photoluminescence (PL) spectroscopy was used to investigate the plasmon-enhanced upconversion photoluminescence by the Au mesoporous films. The upconversion emission spectra of UC nanocrystals deposited on a series of plasmon-enhanced structures under 980 nm laser excitation with a power density of ~ $500\ \mathrm{mW \cdot cm^{-2}}$ are shown in Figure 6.

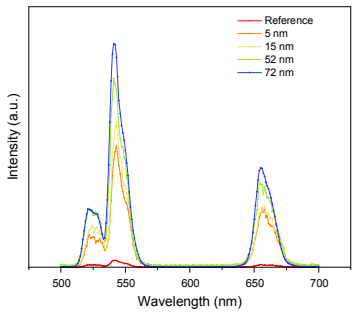

Figure 6. UCPL intensity of β-$NaYF_4$:Yb^{3+}, Er^{3+} NPs on reference substrate and Au mesoporous films with pore sizes of 72 nm, 52 nm, 15 nm and 5 nm, which corresponding to different dealloying time for 8 days, 12 hours, 10 min, and 3 min, respectively.

This figure shows three main emission peaks centred at 520 nm, 540 nm, 660 nm, resulting from $^2H_{11/2} \rightarrow {}^4I_{15/2}$, $^4S_{3/2} \rightarrow {}^4I_{15/2}$, and $^2S_{9/2} \rightarrow {}^4I_{15/2}$ energy transitions in the Er^{3+} rare-earth ions, respectively. It has been previous reported that the effect of plasmonic structures on upconversion can be two competing processes, either enhancement or surface quenching, which is very distance sensitive.[20] The electromagnetic (EM) field strength decays exponentially as a function of inverse forth-power distance away from the plasmonic surface.[21] In our case, UCPL measurement demonstrated a strong quenching effect of UCPL (Figure S7), when UCNPs were deposited directly on mesoporous Au substrates without a spacer layer. In this situation, the emissions of UCNPs relaxed rapidly by nonradiative energy transfer into the surface plasmon resonance. At an optimised distance from the plasmonic surface, fluorescence resonance energy transfer (FRET) from UCNPs to the Au plasmon surface is decreased, while the enhanced EM field can still strong enough to improve the UCPL efficiency. As shown in table 1, it was demonstrated that the PL signals was significantly enhanced on Au mesoporous film samples with 8 nm SiO_2 spacer. The PL intensity of UCNPs on mesoporous Au film with 72 nm averaged pore size, exhibited the best enhancement performance with 32X and 41X enhancement factors, for peaks centred at 541 nm and 656 nm, respectively. There are two main pathways of enhancement: excitation enhancement and emission enhancement. Excitation enhancement indicates the improvement of light absorption of sensitizer ions as a result of the dramatically strengthened local electric field (E) in the vicinity of the surface of plasmonic nanostructure. In parallel, emission enhancement indicates an increase of radiative decay rate of the activator doped in UCNPs, which can be significantly increased due to coupling between electrons and phonons.[26] Theoretical studies show that when a UCNP is located at the vicinity of a metallic structure, an effective coupling exists between the transition dipole of the UCNP and the SPR-induced electric field. The fundamental characteristic of excitation enhancement is that it directly enhances the local field of the UCNPs, thereby causing higher emission intensities without changing the intrinsic characteristics of decay processes. In contrast, emission enhancement occurs due to the increased radiative decay rate, reduced quenching effect and lower localized temperature.[10] In light of these considerations, the observed enhancement in upconversion efficiency can possibly due to both metal-induced enhancement of absorption of the excitation pump at 980 nm (excitation enhancement) *and* plasmonic enhancement of the emission of the UCNPs (emission enhancement).

Published on 19 June 2017. Downloaded by Imperial College London Library on 23/06/2017 03:50:57.

Physical Chemistry Chemical Physics Accepted Manuscript

Please do not adjust margins

View Article Online
DOI: 10.1039/C7CP01959A

Published on 19 June 2017. Downloaded by Imperial College London Library on 23/06/2017 03:50:57.

Table 1. UCPL enhancement factors at 541 nm and 656 nm, with respect to averaged pore size of 5 nm, 15 nm, 52 nm and 72 nm, respectively. Mesoporous substrates have 8 nm SiO_2 spacer layer. Note that the enhancement factors have been corrected based on the densities of the UCNPs on glass and Au film substrates.

Averaged pore size	λ_e =541 nm	λ_e =656 nm
5 nm (3 min)	18	22
15 nm (10 min)	20.9	22.7
52 nm (12 hours)	27.2	32.4
72 nm (8 days)	32	41

Besides the significant enhancement factors, a clear trend was also observed that the UCPL signals were a function of the dealloying time, i.e., with the increase in the mesopore size and the reduction of residual Ag content in the mesoporous film. (Figure 6 and Table 1). After 8 days of dealloying process, the pore size of the mesoporous Au film reached its plateau. The film became unstable and fragile with extended dealloying times longer than 8 days. The increased enhancement factors with increasing pore sizes, indicating significantly increase interaction between electromagnetic waves with mesoporous gold surface at visible/NIR region, is possibly due to increased electromagnetic field enhancement around bigger pores. The plasmon oscillation of the free electrons around the centre of the uniform nanopores can effectively collect and confine light from the near-infrared (NIR) to the visible region into the cavity areas, building up a high density of 'hot spots' in the nanopores,[13,14] suggesting a significant upconversion photoluminescence enhancement is possible due to this electric field enhancement. The random coverage of UCNPs on the mesoporous Au film (Figure 7) means that there is still further potential to improve the enhancement, by adjusting the pore size of the mesoporous Au with respect to the size of UCNPs, as well as the distribution of UCNPs.

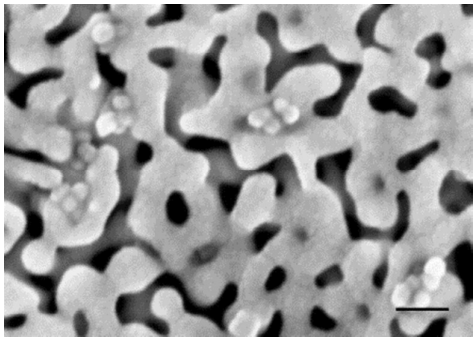

Figure 7. Top-view scanning electron microscopy (SEM) image of the UCNPs sub-monolayer deposited on 72 nm mesoporous Au substrates dealloyed for 8 days. The scalebar in this figure is 100 nm.

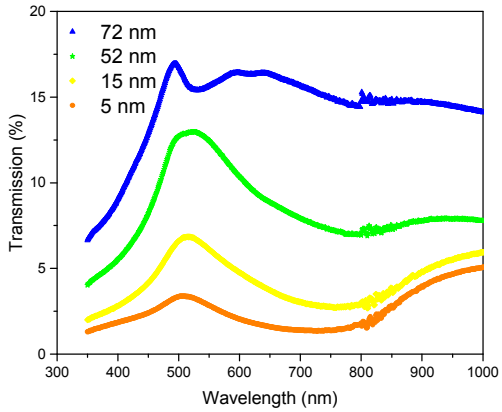

Figure 8. UV-Visible spectroscopy measurement of Au mesoporous films with different pore sizes of 72 nm, 52 nm, 15 nm and 5 nm, which corresponding to different dealloying time for 8 days, 12 hours, 10 min and 3 min, respectively.

To investigate the fundamental optical properties of the mesoporous Au films, UV Visible (UV-vis) spectroscopy measurements was performed on selected mesoporous Au films. Figure 8 shows the UV-Vis transmission spectra corresponding to Au mesoporous films with averaged pore sizes of 5 nm, 15 nm, 52 nm and 72 nm, respectively. Structural imperfections, pore size distribution, surface roughness and residual Ag content may all affect the optical behaviour of Au films. The localised plasmon resonance is observed in all cases at around 530 nm and there is a slight red-shifting with increased pore size. The other observation is that the spectra has a broader band as the pore size increases, indicating a tuneable interaction of the mesopore structures with electromagnetic waves in the broad frequency region. As presented in Figure 8, the transmission of light increased gradually with the increase in the averaged pore size. Clearly, there is a spectral overlap between the 541 nm emission of UCNPs and the UV-Visible spectra of mesoporous films, which may lead to the radiative energy transfer from 541 nm green emission to Au mesoporous film. This energy transfer effect may contribute to the fact that enhancement factors for green emissions (at 541 nm) was slightly weaker than red emissions (at 656 nm), table 1.

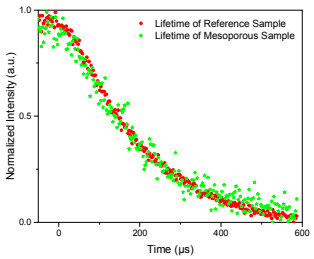

(a)

This journal is © The Royal Society of Chemistry 20xx

Please do not adjust margins

Physical Chemistry Chemical Physics Accepted Manuscript

View Article Online
DOI: 10.1039/C7CP01959A

Published on 19 June 2017. Downloaded by Imperial College London Library on 23/06/2017 03:50:57.

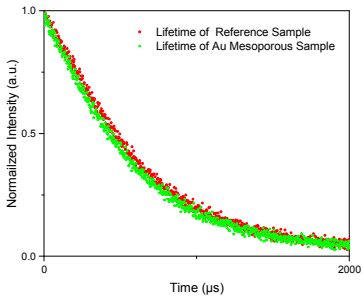

(b)

Figure 9. (a) Time-resolved measurement of the upconversion emission at 541 nm of UCNPs. (b) Time-resolved measurement of the upconversion emission at 660 nm of UCNPs deposited on 12 hours dealloyed mesoporous Au film (Green dots), and UCNPs deposited on the reference sample-clean glass substate (Red dots), respectively.

To further obtain insight of the enhancement mechanism, the change in the decay rate of the UCNP at 541 nm was measured by time-resolved UCPL.[33] The decay times were measured by a series of duration controllable pulsed DeltaDiode laser, and the decay curves were fitted by a DAS6 Analysis software expressed as an exponential function:

$$I=A + B*\exp(-i/T) \quad (1)$$

Table 2. UCPL lifetimes (τ) at 541 nm and 656 nm, with respect to 52 nm mesoporous substrates (12 hours dealloying time) of and the reference sample, respectively.

Wavelength/Sample	τ at 541 nm	τ at 656 nm
Reference Sample	220 μs	506 μs
Mesoporous Sample	212 μs	467 μs

The decay curve is mainly determined by the second excited level of Er^{3+}, as well as the population of the first excited level of Er^{3+} and Yb^{3+}. The green emission (at 541 nm) lifetime measured on the glass substrate and on the mesoporous Au film were 220 μs and 212 μs, respectively. The two similar decay rates measured here (Figure 9a) suggest that the emission enhancement of UCPL at 541 nm was negligible. In contrast, the red emission lifetimes obtained from the reference glass sample and mesoporous Au film sample were 506 μs and 467 μs, respectively. The lifetime of upconversion red emission at 656 nm on mesoporous Au film was calculated to be 39 μs, shorter than its original lifetime exhibited on reference sample. These results suggest that there is negligible enhancement due to the localised surface plasmon resonance. To consider this further electromagnetic modelling using the finite difference time domain (FDTD) technique was carried out.[27,28] The detail of the modelling is included in the supplementary information (Figure S1,S2,S3) but to summarize nanoholes of same diameter as the average nanopores were considered in a periodic array. The holes had a depth or 100 nm and the spacing between adjacent holes was considered to be 40% of the hole diameter. The FDTD results (Figure S1) showed a red shift (505 nm to 547 nm) with increasing nanopore size (5 nm-72 nm) and a widening of the absorbance bandwidth. By considering small dipoles placed above the mesaporous film FDTD calculations also showed insignificant emission enhancement at 541 nm, and a small enhancement (1.4x-2x) dependent on the placement of the emitter at 656 nm (Figure S2). The electromagnetic modelling is in qualitative agreement with the lifetime measurement, in suggesting that the enhancement mechanism is predominantly excitation enhancement and not a plasmonic enhancement of the emission. Further calculated electromagnetic field enhancement at the excitation wavelength for periodic arrays of 72 nm nanoholes shows magnitudes of between 1 and 1.5 in the space above the holes (Figure S2). This leads us to believe that the enhancement is due to the random morphology of the mesaporous surface causing non-resonant enhancement. The exact mechanism will be the subject of future investigation. To further rationalize the observed results of mesoporous Au film enhanced UCPL, one has to consider the intrinsic quantum efficiency of an emitter, Q, which is defined by,[29]

$$Q = k_{rad}/(k_{rad} + k_{nr}) \quad (2)$$

where quantum efficiency is the ratio of the radiative decay rate (k_{rad}) and nonradiative decay rate (k_{nr}). Note that the emitter quantum efficiency is related but not equivalent to the upconversion efficiency.

The UCPL lifetime, which means the average time of excited states spend before relaxations to ground state can be described by equation,

$$\tau = 1/(k_{rad} + k_{nr}) \quad (3)$$

and it is the inverse of the sum of decay rates of all the decay pathways. Hence we can get an alternative equation for quantum efficiency,

$$Q = k_{rad} \cdot \tau \quad (4)$$

Both radiative and nonradiative decay rate can be modified by the presence of the plasmonic surface such as the mesoporous Au film.[30] The plasmonic effect provides extra pathways for UC, alters the emission dynamics and the new UCPL lifetime (τ_0) can be obtained. By comparing steady-state UCPL intensity data and lifetime measurement data between mesoporous sample and reference sample, the enhanced UCPL intensity and decreased lifetime τ_0 at 656 nm indicate an increase of radiative decay rate k_{rad}.[31] On the other hand, the enhanced UCPL intensity but weak change of lifetime at 541 nm suggest negligible decay rate modifications. To understand the plasmonic effect on the pumping power density dependence, the green emission peaked at 541 nm and red emission at 656 nm from the reference sample (UCNPs deposited on clean glass) and the enhanced sample (same amount of UCNPs deposited on 52 nm mesoporous Au substrate) were measured under the same set of excitation power densities, respectively. As a nonlinear effect, the intensity of UCPL (S_{uc}) is simply a function increasing pumping power density (I^n_{pump})

$$S_{up} \propto I^n_{pump} \quad (5)$$

UCPL for both green and red emission are dominated by the energy transfer upconversion (ETU). For both green and red emissions, the luminescence intensity exhibited quadratic dependence (n=2) on the excitation power density at low

Physical Chemistry Chemical Physics Accepted Manuscript

Please do not adjust margins

View Article Online
DOI: 10.1039/C7CP01959A

power regime, and exhibited linear dependence (n=1) at high power regime.[4,6] As a result, the exponent factor n is expected to decrease from 2 to 1 as I_{pump} is tuned from low power to high power. The population of the second excited level will grows large and S_{up} will saturate at extremely high I_{pump}. Upconversion is a non-linear process, which also means that the upconversion quantum yield of the UCNPs itself increases at stronger power densities.[32]

Table 3. UCNPs exponential factor (n) fitted from the 541 nm and 656 nm UCPL emission intensity as a function of excitation power intensities, with respect to UCNPs deposited on 52 nm (12 hours dealloyed) mesoporous samples and UCNPs deposited on the reference sample, respectively.

Wavelength/Sample	541 nm	656 nm
Reference Sample	1.70±0.02	1.88±0.03
Mesoporous Sample	1.70±0.02	1.82±0.05

In table 3, we can see that the exponential factor n of mesoporous Au enhanced sample equals the reference sample (Figure 10(a)), as calculated result shows $n_{Au} = n_{ref}$=1.70±0.02, where the power dependence of the log(I_{pump})-log(S_{uc}) are consistent for both substrates in the low pumping power limit (below 5.35 W/cm^2). Again, consistent with the negligible changed lifetime at green emission (541 nm), the unchanged exponential factor n further confirmed that the enhancement mechanism of UCPL at 541 nm was mainly due to excitation enhancement. While the exponential factors at 656 nm red emission calculated from reference sample is 1.88 ±0.03 and 1.82 ±0.05 from mesoporous enhanced sample, respectively (Figure 10(b)). The slightly reduced exponent factor agrees well with the slightly decreased lifetime (39 μs), as well as the higher enhancement factor at red emission (656 nm) compared with that at green emission (541 nm). Alternatively, the UCPL enhancement at 656 nm channels suggest the contributions of both excitation enhancement and emission enhancement.

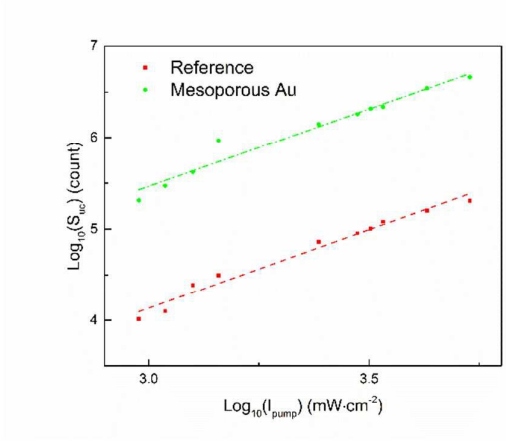

(a)

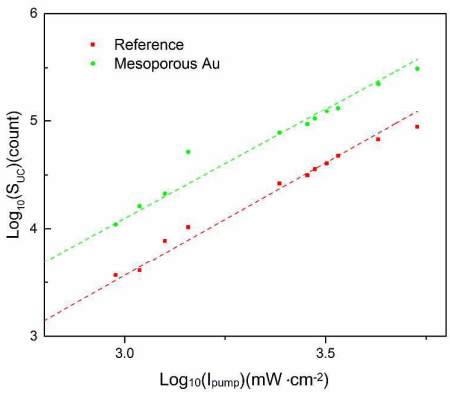

(b)

Figure 10. (a) Green (541 nm) luminescence intensity of UCNPs as a function of increasing pumping power density of the UCNPs deposited on the 52 nm mesoporous Au sample (Green line) and UCNPs deposited on the reference sample-clean glass substate (Red line), respectively. (b) Red (656 nm) luminescence intensity of UCNPs as a function of increasing pumping power density of the UCNPs deposited on the 52 nm mesoporous Au sample (Green line) and UCNPs deposited on the reference sample-clean glass substate (Red line), respectively.

4. Conclusions

In summary, 3D mesoporous Au film fabricated by a dealloying process was prepared and optimized by tuning their pore sizes with respect to dealloying times. These films induced significant enhancement of UCPL of β-$NaYF_4$:Yb^{3+}, Er^{3+} co-doped nanocrystals, with significant enhancement over a large uniform area, with constant enhancement factor for low pumping power density. The UCPL enhancement measurements and the time-resolved UCPL study indicate that enhanced UCPL is dominated by the excitation enhancement at 541 nm, and a combination of excitation enhancement and emission enhancement at 656 nm. The high emission intensity enhancement, together with other fascinating advantages, such as low-cost, high throughput and reproducibility, make the plasmonic 3D mesoporous Au film platform an excellent candidate for realizing high efficiency of UCPL.

Author Contributions

H.Qin carried out upconversion nanoparticle synthesis, characterization, and plasmonic enhanced upconversion investigation. H.Qin prepared the first draft of the manuscript. A.Shamso prepared mesoporous gold films and characterization. I.Theodorou and A. Mihai helped plasmonic substrate preparation. A.Centeno carried out electromagnetic modelling and contributed to the discussion. M.P.Ryan and F.Xie conceived the research ideas. F.Xie supervised the project. All authors have given approval to the final version of the manuscript.

Acknowledgements

This journal is © The Royal Society of Chemistry 20xx

Published on 19 June 2017. Downloaded by Imperial College London Library on 23/06/2017 03:50:57.
Physical Chemistry Chemical Physics Accepted Manuscript
Please do not adjust margins

View Article Online
DOI: 10.1039/C7CP01959A

The authors acknowledge the support from the Department of Materials Thin Film Lab, Imperial College London.

References

1 Y.-L. Wang, N. Mohammadi Estakhri, A. Johnson, H.-Y. Li, L.-X. Xu, Z. Zhang, A. Alù, Q.-Q. Wang and C.-K. Shih, Scientific Reports, 2015, 5, 10196.
2 T. Trupke, M. A. Green and P. Würfel, Journal of Applied Physics, 2002, 92, 4117-4122.
3 Deepak V, Saetre T, Midtgard O. 2012, 38th IEEE Photovoltaic Specialists Conference. 2012
4 D. Lu, S. K. Cho, S. Ahn, L. Brun, C. J. Summers and W. Park, ACS Nano, 2014, 8, 7780-7792.
5 X. Chen, W. Xu, H. Song, C. Chen, H. Xia, Y. Zhu, D. Zhou, S. Cui, Q. Dai and J. Zhang, ACS Applied Materials & Interfaces, 2016, DOI: 10.1021/acsami.5b12528.
6 W. Zhang, F. Ding and S. Y. Chou, Advanced Materials, 2012, 24, OP236-OP241.
7 Z. Xu, M. Quintanilla, F. Vetrone, A. O. Govorov, M. Chaker and D. Ma, Advanced Functional Materials, 2015, 25, 2950-296
8 A. Priyam, N. M. Idris and Y. Zhang, Journal of Materials Chemistry, 2012, 22, 960-965.
9 M. Saboktakin, X. Ye, S. J. Oh, S.-H. Hong, A. T. Fafarman, U. K. Chettiar, N. Engheta, C. B. Murray and C. R. Kagan, ACS Nano, 2012, 6, 8758-8766.
10 M. Saboktakin, X. Ye, U. K. Chettiar, N. Engheta, C. B. Murray and C. R. Kagan, ACS Nano, 2013, 7, 7186-7192.
11 F. Wang, J. Wang and X. Liu, Angewandte Chemie International Edition, 2010, **49**, 7456-7460.
12 Z. Li, L. Wang, Z. Wang, X. Liu and Y. Xiong, The Journal of Physical Chemistry C, 2011, 115, 3291-3296.
13 C. Li, Ö. Dag, T. D. Dao, T. Nagao, Y. Sakamoto, T. Kimura, O. Terasaki and Y. Yamauchi, Nat Commun, 2015, 6.
14 Z. Yi, J. Luo, X. Tan, Y. Yi, W. Yao, X. Kang, X. Ye, W. Zhu, T. Duan, Y. Yi and Y. Tang, Scientific Reports, 2015, 5, 16137.
15 C. Noguez, The Journal of Physical Chemistry C, 2007, 111, 3806-3819.
16 Y. Ding, Y. J. Kim and J. Erlebacher, *Advanced Materials*, 2004, **16**, 1897-1900.
17 X. Wang, Z. Qi, C. Zhao, W. Wang and Z. Zhang, The Journal of Physical Chemistry C, 2009, 113, 13139-13150.
18 C. J. Dotzler, B. Ingham, B. N. Illy, K. Wallwork, M. P. Ryan and M. F. Toney, Advanced Functional Materials, 2011, 21, 3938-3946.
19 E. J. Schofield, B. Ingham, A. Turnbull, M. F. Toney and M. P. Ryan, Applied Physics Letters, 2008, 92, 043118.
20 A. L. Feng, M. L. You, L. Tian, S. Singamaneni, M. Liu, Z. Duan, T. J. Lu, F. Xu and M. Lin, Scientific Reports, 2015, 5, 7779.
21 W. Xu, Y. Zhu, X. Chen, J. Wang, L. Tao, S. Xu, T. Liu and H. Song, Nano Research, 2013, 6, 795-807.
22 F. Wang, R. Deng and X. Liu, *Nat. Protocols*, 2014, **9**, 1634-1644. X.
23 Li, R. Wang, F. Zhang and D. Zhao, *Nano Letters*, 2014, **14**, 3634-3639.
24 Y. Hashimoto, G. Seniutinas, A. Balčytis, S. Juodkazis and Y. Nishijima, Scientific Reports, 2016, 6, 25010.
25 M. Wahl, H.-J. Rahn, I. Gregor, R. Erdmann and J. Enderlein, Review of Scientific Instruments, 2007, 78, 033106.
26 G. Chen, C. Ding, E. Wu, B. Wu, P. Chen, X. Ci, Y. Liu, J. Qiu and H. Zeng, The Journal of Physical Chemistry C, 2015, 119, 22604-22610.
27 A.F.Oskooi, D.Roundy, M.Ibanescu, P.Bermel, J.D.Joannopoulos and S.G.Johnson, Computer Physics Communications, 20120, 181, 687-702.
28 A. Centeno, N. Alford and F. Xie, IET Nanobiotechnology, 2013, 7, 50-58.
29 D. M. Wu, A. García-Etxarri, A. Salleo and J. A. Dionne, *The Journal of Physical Chemistry Letters*, 2014, **5**, 4020-4031.
30 A. Camposeo, L. Persano, R. Manco, Y. Wang, P. Del Carro, C. Zhang, Z.-Y. Li, D. Pisignano and Y. Xia, *ACS Nano*, 2015, **9**, 10047-10054.
31 N. S. Abadeer, M. R. Brennan, W. L. Wilson and C. J. Murphy, *ACS Nano*, 2014, **8**, 8392-8406.
32 G. Chen, H. Qiu, P. N. Prasad and X. Chen, Chemical Reviews, 2014, 114, 5161-5214.

Published on 19 June 2017. Downloaded by Imperial College London Library on 23/06/2017 03:50:57.

Physical Chemistry Chemical Physics Accepted Manuscript

Please do not adjust margins